Cement and Concrete Composites 74 (2016) 191–200

Contents lists available at ScienceDirect

Cement and Concrete Composites

journal homepage: www.elsevier.com/locate/cemconcomp

An improved image processing method for assessing multiple cracking development in Strain Hardening Cementitious Composites (SHCC)

Cong Lu*, Jing Yu, Christopher K.Y. Leung

Department of Civil and Environmental Engineering, HKUST, Clear Water Bay, Kowloon, Hong Kong

ARTICLE INFO

Article history:
Received 1 October 2015
Received in revised form
29 June 2016
Accepted 1 October 2016
Available online 4 October 2016

Keywords:
SHCC
Crack detection
Crack width
Fiber distribution

ABSTRACT

Strain Hardening Cementitious Composites (SHCC) exhibit tension-hardening behavior accompanied by the formation of multiple cracks. To study the multiple cracking process, cracks are identified from digital images. As conventional image processing technique based on a single threshold of gray intensity cannot accurately determine the width of both fine and wide cracks, a new double-threshold algorithm is developed and its accuracy is verified by comparing with direct measurement under the microscope. Then, an additional algorithm for removing the noises and isolating individual crack regions is introduced. With the improved image processing method applied to a large number of sequential images, detailed information on the development of crack number and width is acquired. The average value and deviation of crack width at a given strain can be calculated to facilitate durability design. Also, with the stress-crack width relation obtained for various cracks, the fiber distribution among cracked sections can be estimated.

1. Introduction

Under tensile loading, cementitious materials often fail by the formation of a localized crack, with the stress vs strain relation showing a rapidly dropping softening branch after the strength is reached. To reduce the brittleness of the failure, fiber reinforcement can be incorporated. Based on micromechanical models that provide guidelines for selecting the properties of fiber, matrix and fiber/matrix interface [1–4], strain hardening cementitious composites (SHCC) can be made with short random fibers at volume fraction of 2% or below. For SHCC under direct tension, the strain hardening regime can extend to a strain level of several percent. In contrast to other cementitious materials (including conventional fiber reinforced concrete or mortar) which fail in tension with the opening of a single crack, failure in SHCC is accompanied by the formation of multiple fine cracks at small spacing. The opening of each crack can be controlled to below 60 μm even at very high strain [5]. In structural applications, members made with SHCC exhibit high ductility and energy absorption. In addition, durability of the member can be significantly improved as the tight control of crack opening enables the material to maintain its resistance against water and chemical penetration under practical loading conditions [6,7].

To assess the enhanced performance of SHCC, the direct tensile test is usually performed with a dog-bone shaped specimen or rectangular coupon specimen to obtain the stress vs strain behavior up to the ultimate strength, after which deformation will localize into a single crack and the stress starts to decrease. The test result can reflect the strength, ductility and energy absorption of the material but does not offer information on the cracking situation. For example, the same strain can be resulted from the relatively wide opening of a small number of cracks or the controlled small opening of a large number of cracks. In terms of durability, the latter is much more desirable. Actually, to characterize the transport properties (such as water permeability and chloride diffusivity) of SHCC under loading, it is necessary to know the crack spacing and opening at a particular strain level. As the relation between transport properties and crack opening is not linear, the distribution of crack opening, rather than the average value, also needs to be obtained.

Information on the crack opening at a particular strain can be obtained with a two-step approach. The relation between applied tensile stress and opening of a single crack is first determined. Then, for a SHCC member under a particular stress, the crack opening is

* Corresponding author.
E-mail address: cluab@ust.hk (C. Lu).

http://dx.doi.org/10.1016/j.cemconcomp.2016.10.005
0958-9465/

known while the crack spacing is determined from an analysis of stress transfer from the crack back to the matrix (through the fiber/matrix interface) [8,9]. Knowing the crack opening and spacing, the strain can be determined. If a sufficient number of stress vs crack opening curves have been experimentally measured, different properties can be statistically assigned to different cracks along the member to enable more realistic simulation of the cracking process.

Experimental determination of the tensile stress-crack opening relation in SHCC has been conducted in Ref. [10]. To generate a single crack in SHCC which normally exhibits multiple cracking behavior, a thin notch was inserted in the middle of the specimen to reduce the cross-section. From the test results, a crack width of over 500 μm was observed at peak stress for PVA-SHCC. However, according to calculations from fiber bridging models with and without the consideration of fiber rupture [1,11], the crack width at peak stress is normally less than 200 μm. Additionally, inspection of un-notched specimens under direct tension revealed that the width of each localized crack is far smaller than 500 μm [5]. It is therefore suspected that the tensile test with a thin notch may not be able to generate a perfect single crack. We therefore carry out tensile testing on a notched specimen in a manner similar to [10]. A SHCC with 2.5% PVA fiber is employed. The crack opening at maximum stress is also found to be slightly more than 500 μm. After the test, a slice of material adjacent to the notch is cut out to reveal the cracking inside the sample. As shown in Fig. 1, multiple cracks can be observed within a region next to the notched section. This is because the stress is decreasing gradually away from the notched section (rather than showing a sudden drop between the unnotched and notched parts which will violate equilibrium). As the material hardens after cracking occurs at the notch, the transfer of stress by the fibers to the region adjacent to the notch can result in additional cracking. These additional cracks can contribute to the measured opening, as the gauge length of the instrument is often much larger than the crack spacing.

In view of the difficulty in ensuring the formation of a single crack in SHCC, even with the use of a notched specimen, a better approach is to assess the crack bridging behavior directly from each of the multiple cracks formed in an un-notched specimen. To fulfill this objective, optical measurement methods can be employed. In Ref. [12], a digital image correlation (DIC) system with two 3D cameras was used to measure the displacement in small sub-regions on the surface of a specimen under direct tension. Then the cracks were determined from the locations where the relative displacement increases greatly between two sub-regions along the direction perpendicular to the cracks. Admittedly, DIC is a precise method since it determines the displacement field. However, the equipment and software for DIC system are very costly and the experimental setup is very complicated so the method cannot be adopted in normal laboratories. Besides, DIC algorithm requires partitioning the image into small sub-regions. For SHCC, since the cracks are very close to one another, the sub-region needs to be made very small so each region will not contain more than one crack. This can make the computation highly inefficient and time-consuming, especially if the crack openings at many different strain levels (and times) need to be determined.

The present study will focus on the development of a Digital Image Processing (DIP) method to study the multiple cracking process. In DIP, images of cracking patterns can be taken with a normal camera for analysis, which is much simpler and more feasible. DIP method has been adopted in Refs. [13,14] for the study of SHCC. To save work, the cracking patterns were only recorded at a few strain levels (0.5%, 1.0%, 1.5%, 2.0%, 2.5%, 3.0%, 3.5%, and 4.0% in Ref. [13]). In the analysis, several lines perpendicular to the cracks were inserted in each image (Fig. 2), after which the crack widths and crack number were measured and counted at the intersection points of the lines and cracks (observation points). With this approach, there are two major limitations in obtaining complete information on cracking patterns: 1) the observation points need to be assigned manually on the cracks in every image since points on cracks cannot be automatically distinguished from noises (blemishes on specimen surface for instance) with similar gray intensity; 2) the widths of cracks at observation points need to be measured by counting pixels individually. As the analysis of image has to be manually performed, only a relatively small number of images can be studied and the number of observation points on each image also has to be limited. Otherwise the workload for the image processing would be impractically intensive. In the case when pictures were taken at large strain intervals such as 0.5% in Ref. [13], cracking information will be missed at smaller strain level (such as 0.1%, 0.2%, etc.) which are commonly encountered in concrete structures under serviceability state. Besides, the cracking pattern is often very complicated and the width along a crack can vary quite significantly, especially for cracks that do not run through the whole section (Note: the opening of such cracks is zero at its tip). The average crack width measured at a few observation points is not sufficiently accurate. The above discussions reveal the need to develop an approach that can automatically distinguish cracks, noises and background in a large number of images, extracts the

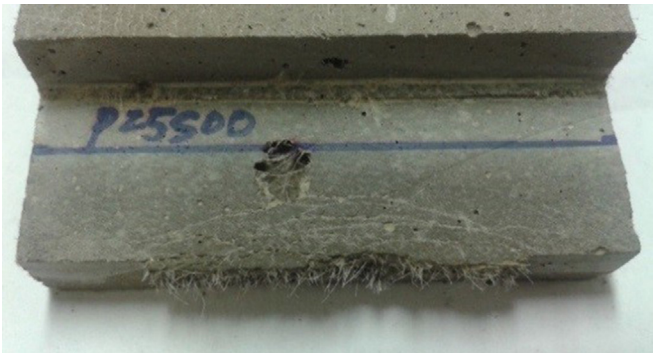

Fig. 1. Cutting of tested notched sample.

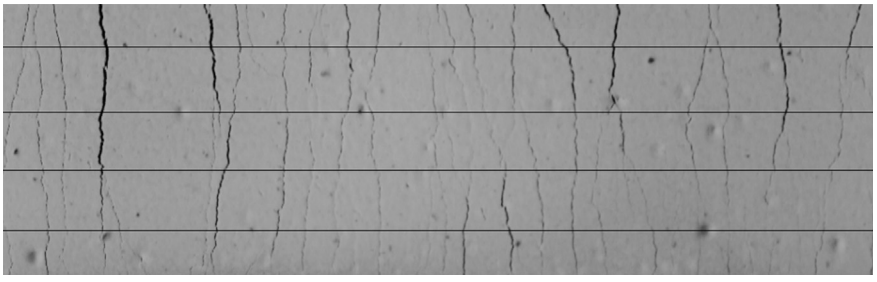

Fig. 2. Several horizontal lines were inserted in each image for image processing.

cracks from each image and determine important parameters related to the cracks (such as total crack length, mean and standard deviation of crack width, etc.).

This study aims at developing a digital image processing method to investigate the number and opening of multiple cracks in SHCC at arbitrary strain levels. A new algorithm for distinguishing cracks from the background, particularly suitable for SHCC material, is proposed. Traditionally, the cracks are detected by setting a threshold of gray intensity. For the case of SHCC, some of the fine cracks are not sufficiently dark to be detected with a high threshold, while wider cracks will be artificially expanded if a low threshold is employed. To address this issue, a double-threshold algorithm is developed to capture both wide and fine cracks. To verify the accuracy of the approach, crack widths obtained from the digital image of a multiple-cracked sample are compared directly to measurements under the optical microscope. Then, another algorithm for removing the noises and isolating individual cracks (or crack regions) will be introduced. To illustrate the application of this post-processing algorithm, the development of crack number and widths in a specimen under direct tensile loading is presented. At any given strain, the average crack width and its standard deviation are obtained. With this information, the probability for the crack width to exceed a critical value can be easily calculated. Through the use of a theoretical model, the variation of fiber content, which is an important factor governing the variation in SHCC strength and ductility, will also be derived.

2. Experimental program

2.1. Preparation of specimens

The aim of this study is to quantitatively assess the multiple cracks generated when SHCC is under direct tension. Uniaxial tensile test of SHCC was therefore performed on rectangular specimens and crack patterns on one of the surfaces were photographically recorded. To prepare test specimens, the mix proportion shown in Table 1 was employed. After the casting and curing for 28 days, the ends of the specimen were reinforced with carbon fiber reinforced polymer and aluminum plates to prevent failure from stress concentration. Also, to provide a smooth surface which will show sharp edges with good differentiation between the features of interest (multiple cracks in this study) and the surrounding matrix, different colors of paint have been applied on the surface to increase the contrast. After preliminary trials, a yellow paint was found to be most effective.

2.2. Setup of tensile test

The uniaxial tensile test was performed under displacement control on a standard 810-Material Testing Machine. Both ends of the sample were gripped in the machine and tensile loading was applied at a displacement rate of 0.1 mm/min.

Since the cracks in SHCC are very fine, especially at their initiation stage, it is desirable to have as many pixels as possible in the captured image in order to improve measurement precision. With this objective, a macro lens with magnification of 1:1 was used, to take a photograph of an area on the side of the specimen, which was 36 mm along the tensile loading direction and 15 mm in width. The camera used in the test is equipped with a full-frame CMOS sensor with size of 35.9 mm × 24 mm, and resolution of 6016 × 4016. With a tripod, the camera was placed in front of the MTS machine (Fig. 3) and the distance between the CMOS image sensor in the camera and the sample surface was roughly 0.35 m while the size of view field was about 42 mm × 28 mm. With this arrangement, the size of a single pixel in the photo corresponded to around 7 μm in reality. After the focus was placed manually at the surface of sample, a remote timer was used to take one photo every 20 s.

Table 1
Mix proportion for SHCC.

Cement	Fly ash	Silica fume	Sand	Water	SP	PVA fiber
0.18	0.8	0.02	0.2	0.2	0.44%	2.5%

3. Image processing algorithm

After the images have been obtained, the cracks have to be detected for the measurement of length and width. In this section, a computer algorithm for isolating the cracks from the surrounding cementitious matrix and eliminating the noise in the image is presented.

3.1. Background correction

The original images were first converted from RGB images to gray images by averaging the red, green and blue signals (Fig. 4). As shown in Fig. 4, the cracks appear to be darker than the surrounding matrix.

After obtaining the gray image, subtraction pre-processing was carried out to remove slight variations due to irregularly illuminated conditions and shading [15]. In the processing, a smoothed image (Fig. 5a) was obtained by applying the median filter to remove thin line structures associated with cracks. This smoothed image (Fig. 5a) was then subtracted from the gray image in Fig. 4 to obtain a background corrected image (Fig. 5b).

3.2. Segmentation of cracks

The background corrected image Fig. 5b is still a gray image for which the cracks and background remain undistinguished. To detect cracks automatically by the computer, the key is to convert the background corrected gray image (Fig. 5b) into binary image where the values of pixels on cracks are denoted as 1 (white) while the other pixels are 0 (black).

To come up with a binary image, a thresholding process is normally used, with '1' assigned to pixels with gray intensity above a certain threshold and '0' assigned to the rest. Fig. 6a shows the

Fig. 3. A camera is placed in front of the specimen to capture crack patterns.

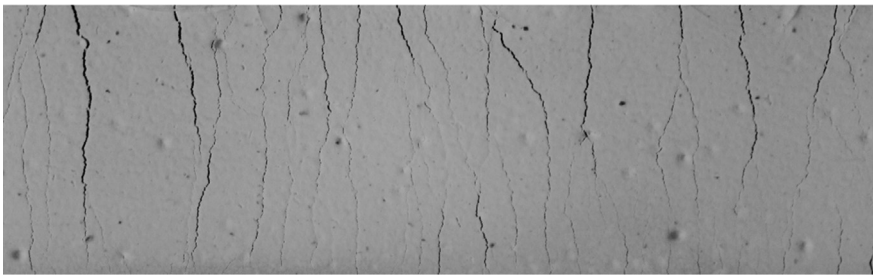

Fig. 4. Gray image.

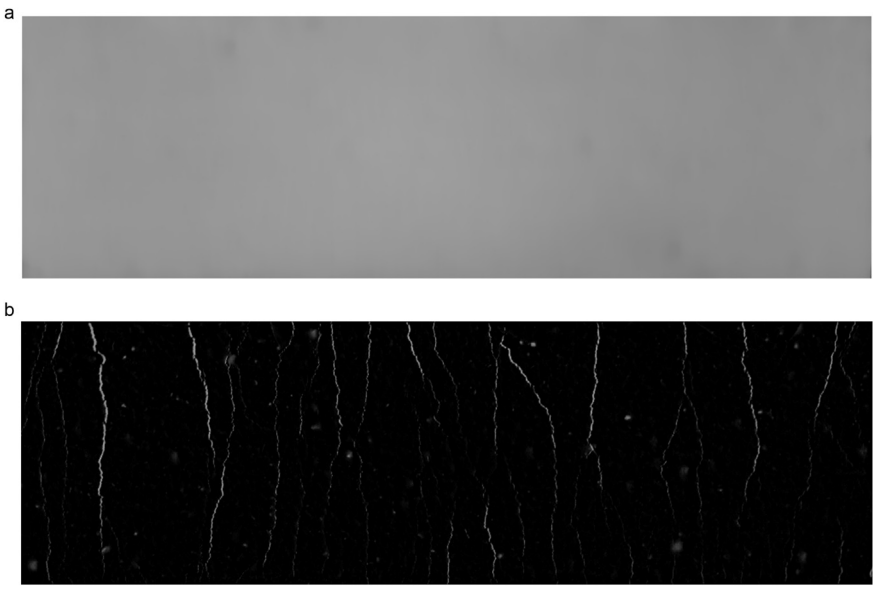

Fig. 5. a) Smoothed image using median filter; b) background corrected image.

original gray image from which one can tell the actual width of the crack. The major challenge in this approach is to determine the proper threshold intensity to yield the binary image that shows the same width as in the original image. On one hand, if a high threshold (e.g., 0.25) is used, as in Fig. 6b, the width of wide crack in the upper part will be accurately presented but the fine cracks in the lower part will become invisible as they are not as dark in the original image and have a smaller gray intensity. On the other hand, if a lower threshold (e.g., 0.08) is used (Fig. 6c), the fine cracks will be accurately captured but the width of wide crack will be artificially expanded to become larger than the actual value.

To eliminate the above shortcomings of thresholding, a new double-threshold algorithm is proposed in this study. With this algorithm, Fig. 6b and c can be combined to reveal correct widths for both wide and fine cracks. The flow chart for the algorithm is shown in Fig. 7.

A higher threshold and a lower threshold are first applied to obtain the two images shown in Fig. 6b and c. As mentioned before, the width of wide crack in the upper part of the image is correctly

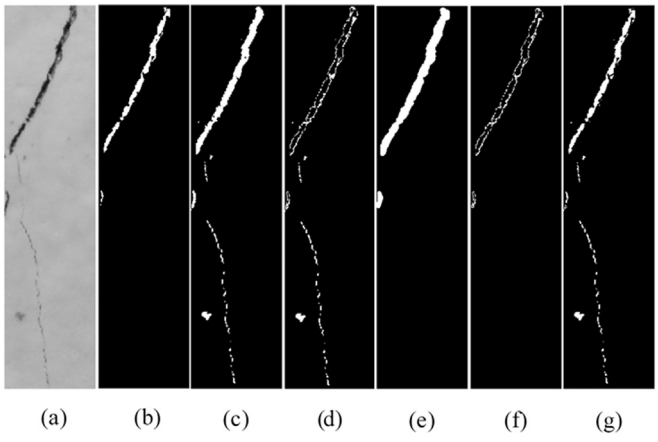

Fig. 6. Schematic for image processing using double-threshold algorithm.

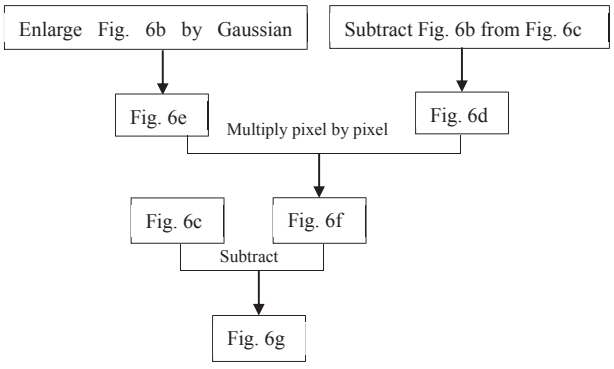

Fig. 7. Flow chart double-threshold algorithm.

presented in Fig. 6b but the fine crack in the lower part is missing. On the contrary, in Fig. 6c, the fine crack is correctly captured but the wide crack is artificially enlarged.

To correctly capture both wider and fine cracks, several additional steps are required. By subtracting Fig. 6b from Fig. 6c, the image in Fig. 6d, which includes the fine crack in Fig. 6c as well as the extra artificial boundary of the wide crack, is obtained. In reality, the artificial boundary is not part of the wide crack and should therefore be eliminated. To do so, a filter based on the Hessian matrix and Gaussian filter adopted in Ref. [15], which can emphasize and enhance lines, is applied on Fig. 6b to enlarge the area of the wide crack, giving the image in Fig. 6e. Then the matrices of images (in the form of '1's and '0's) in Fig. 6d and e are multiplied pixel by pixel. In this step, only overlapped non-zero pixels in the two figures will yield a non-zero product and hence be reserved. As a result, everything except the extra boundary in Fig. 6d is eliminated (as in Fig. 6f).

As a last step, the boundary in Fig. 6f is subtracted from Fig. 6c, to correct the width of wide crack in Fig. 6c to the real width in Fig. 6b. Consequently, the final binary image (Fig. 6g) accurately presents both the wide crack in Fig. 6b and the fine crack in Fig. 6c. It should be pointed out that there are still noises in the image that need to be further addressed. However, before doing so, we would first compare the crack widths in the processed image to those obtained from direct optical measurements.

3.3. Verification of crack width by direct measurement with microscope

In the processed binary image (Fig. 6g), the cracks are presented as a collection of pixels. As the size of one pixel is known, the widths of each crack at a particular location can be obtained by counting the number of pixels on it along the loading direction. To verify the reliability of this processing method, a photograph of a tested specimen was taken after it was unloaded (Fig. 8a). It was then processed into a binary image following the approach described above. A horizontal line (as shown in Fig. 8a) was defined in the picture and the crack opening was determined for each of the 14 points where the horizontal line intersected with a crack. The unloaded specimen was also placed under an optical microscope (Olympus BH-2), and digital images were taken with a Leica DFC480 camera mounted over the ocular lens, so the crack opening at the same points can be measured with a software in the computer. Fig. 8b shows the photograph at a particular crack captured by the microscope which has a pixel size of 0.168 μm. As shown in Fig. 8b, the crack width at the point intersected by the horizontal line in Fig. 8a was measured to be 33.4 μm. The comparison of crack width determined from the microscope and the binary image is shown in Fig. 9. The results are mostly within about 10 μm from one another. The difference is resulted from the fact that the crack width in the binary image is a whole number multiple of the pixel

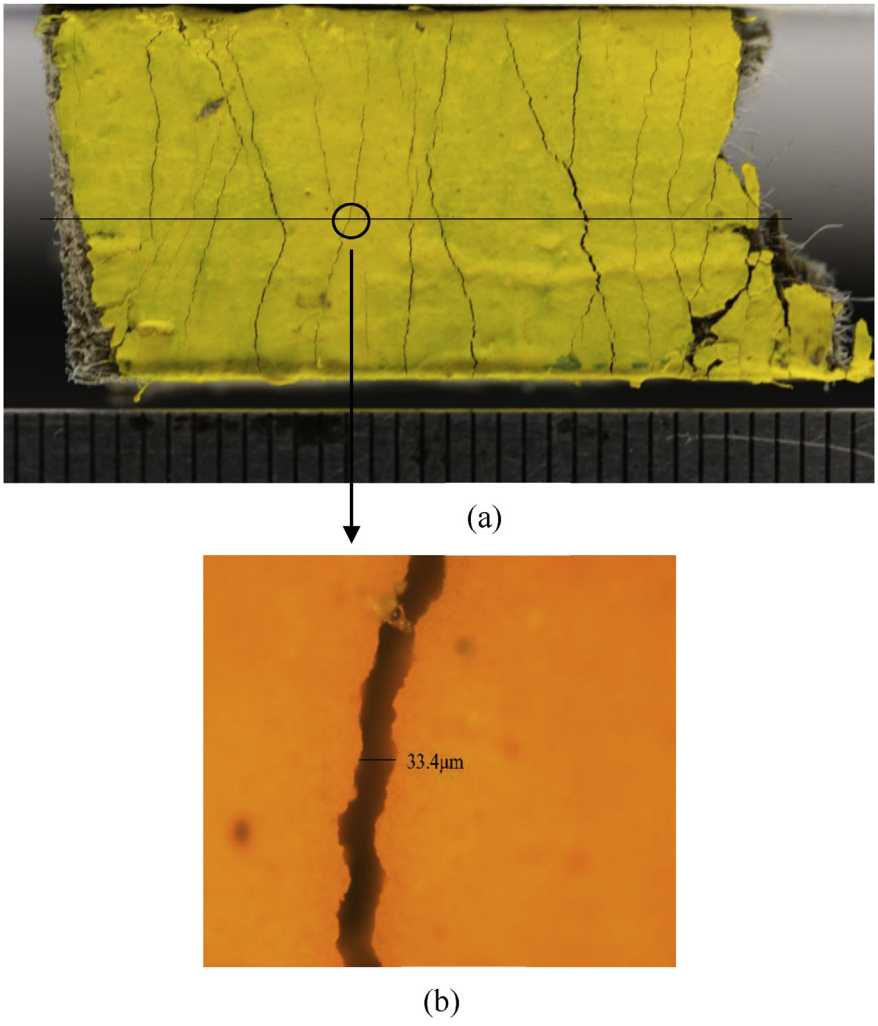

Fig. 8. a) Image of the whole specimen; b) image taken by microscope.

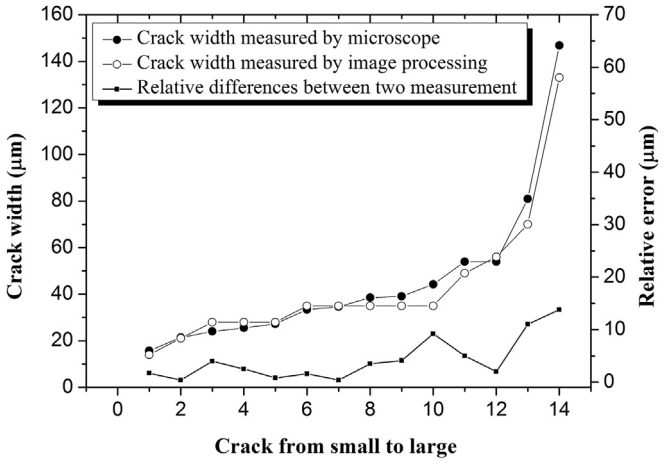

Fig. 9. Comparison of crack width from image processing and microscope.

size, which is several microns, as the resolution is not as high as that of the optical measurement. Besides, the pre-set thresholds have certain influence on the accuracy. In the algorithm, there are two measurements for each point, one from higher threshold and the other from lower threshold. In the processed image, the suitable measurement for each crack, which is closer to actual value, is chosen according to the following principles: fine crack takes the measurement from lower threshold while wide crack takes the measurement from higher threshold. From the graph, it can be found that the wide cracks tend to show larger error. This is caused by the fact that the width of wide cracks covers several tens of pixels and the boundaries of them show a gradual change from higher grayscale to lower. It could therefore be more difficult to recognize the exact boundaries of wide cracks and therefore the errors tend to be larger.

In our opinion, as long as the error for a single point is within 2 pixels (14 μm), the precision is sufficient for the assessment of the crack width especially when the average width along a certain crack is to be determined, as the averaging should reduce the error caused by lower resolution (which results in over-estimation at some points and underestimation in others). To demonstrate this, 16 points were taken on a certain crack at uniform spacing. The crack opening at each point was measured both from the processed image and directly under the microscope. Comparing the 16 pairs of measurements, the average absolute error was 5.72 μm. When the widths at two consecutive points were averaged first (so there were 8 pairs of 'averaged' values), the average absolute error reduced to 3.33 μm. By averaging the widths for 4, 8 and all 16 points first, the average absolute errors became 2.7 μm, 2.7 μm and 0.975 μm respectively, indicating that the error of the image processing can be reduced greatly by taking the average width for all the points along a crack (which can be easily performed with a computer program). Also, with the advance in photographic equipment, the resolution of image sensors is expected to increase. Using the same algorithm developed in this work, higher precision can be obtained.

3.4. Elimination of noises

As mentioned in Section 3.2, the binary image obtained from the

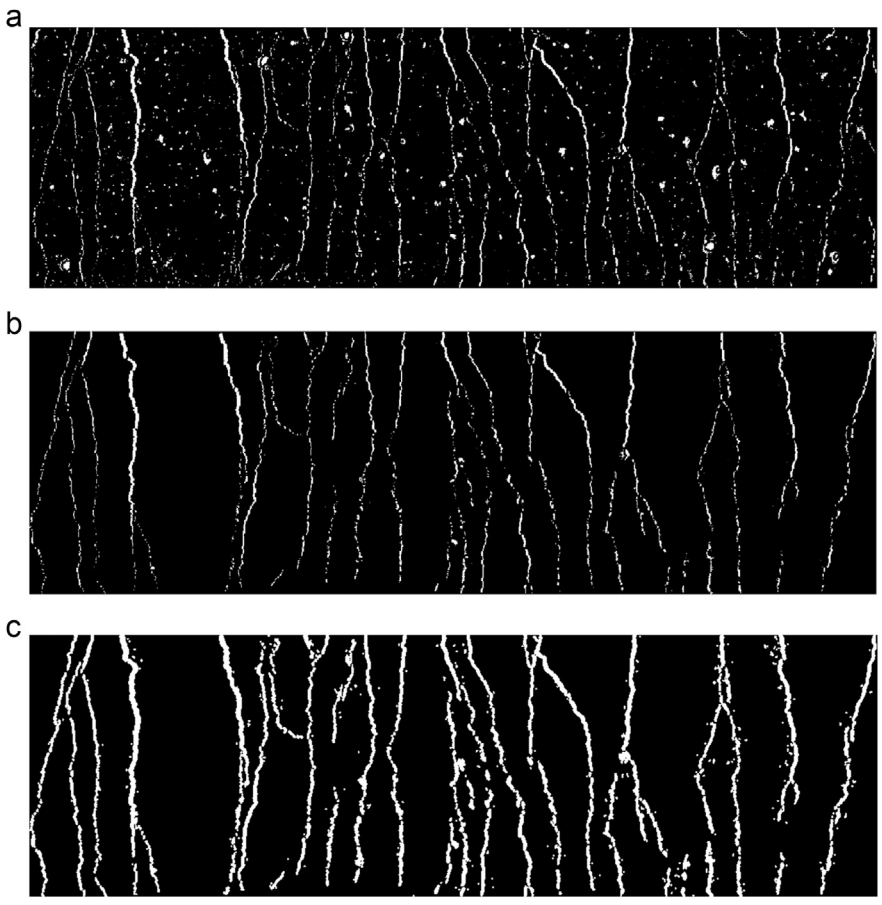

Fig. 10. a) Binary image; b) last image with noises eliminated manually; c) enlarged image using Gaussian filter.

algorithm in Fig. 7 is still 'contaminated' with noises. An example of such image is shown in Fig. 10a. If a large number of images taken at different times are to be studied, removing the noise from each image manually will become very tedious. An automated approach was hence developed. With the help of the commercial software Photoshop CS6, all the noises were manually eliminated on the last image which was taken at the very end of the test (Fig. 10b). (Note: this is the only image that needs to be handled manually.) Then an enlarged image of Fig. 10b was generated by applying the Gaussian filter (Fig. 10c).

The enlarged image in Fig. 10c was then multiplied with the second last image. Because only the overlapping non-zero pixels which make up cracks were reserved, the noises on the second last image were also eliminated (Fig. 11). Then, by enlarging Fig. 11 with the Gaussian filter, and multiplying it with the third last image, the noises in the latter would be removed. The above process is applied iteratively, so starting from the last image, images at all previous stages could be 'denoised' one by one.

3.5. Separation and tracking of cracking region

To evaluate the variation of behaviors among different cracks, individual cracks should be separated from each other. It is commonly observed during testing that several cracks may join into one crack or one crack may branch off into several cracks (as shown in Fig. 12b). It is therefore difficult to define and track an individual crack. In this study, the evaluation of cracking behavior will be conducted among divided cracking regions, which are defined as either 1) a single crack when the crack stays clear from others (Fig. 12a), or 2) closely located which tends to intersect, or cracks generated as branches of a single initial crack (Fig. 12b).

The identification and separation of cracking regions are manually performed in Photoshop on the last image only. Then, an image expansion (through Gaussian filter) and multiplication method similar to that described in the last subsection is used to identify pixels in the same cracking regions on the second last image. Through an iterative process, individual crack regions (such as the one in Fig. 13) are extracted from each image. The propagation and opening of crack(s) in each region during the loading process can then be traced.

3.6. Determination of crack number and crack width

From the binary image of each cracked region, the total area occupied by the pixels as well as the boundary coordinates of each part of the crack can be easily determined. In this study, the crack length is taken to be the length projected onto a plane perpendicular to the loading direction. For each part of the crack, it is calculated from the corresponding coordinate values at its boundaries. The total crack length in each crack region is simply the sum of lengths of all parts. Dividing the total area of the pixels by the total length, the average crack width within the region is obtained. To find the number of cracks along the whole specimen, the total length of cracks in all the cracking regions are added together and divided by the width of the member. The crack number is then a non-integer, which is perhaps a more realistic representation of the situation where the branching and joining of cracks are commonly observed.

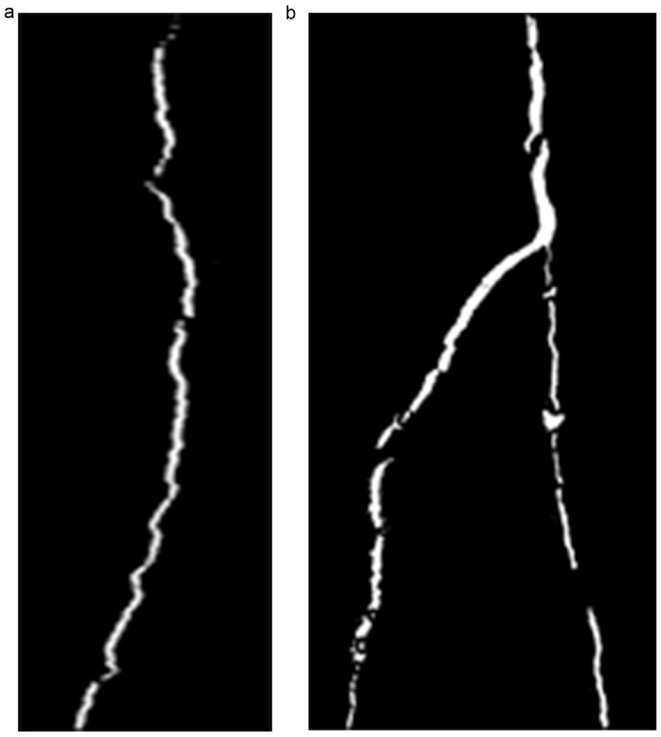

Fig. 12. a) Single crack that stays clear from other cracks; b) one crack that branches off into two cracks.

4. Results and discussion of image processing on SHCC

In this section, we will focus on the processed images from a single SHCC specimen to demonstrate how various useful information regarding the multiple cracking process can be obtained from a single tensile test.

4.1. Crack number development

As discussed in the above section, the number of cracks along the observed part of the specimen can be obtained from the processing of each image which corresponds to different stress levels. The result of crack number vs applied stress is shown in Fig. 14.

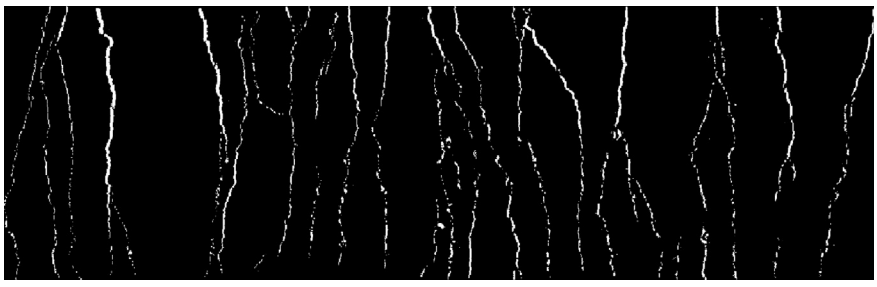

Fig. 11. Processed last but one image with noises eliminated.

Fig. 13. A crack region separated from the others.

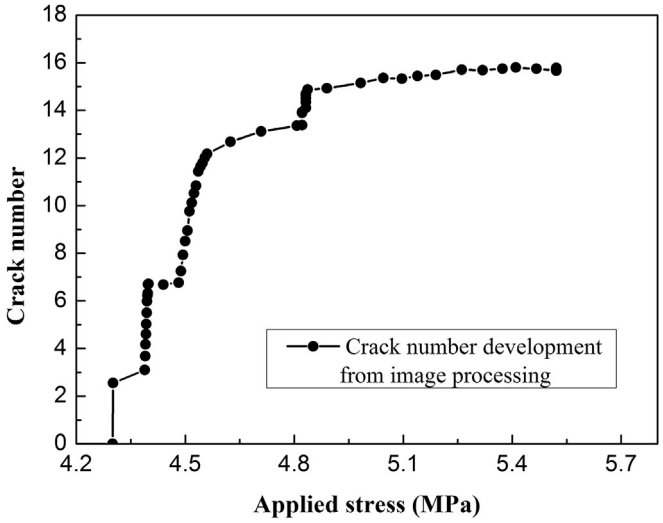

Fig. 14. Crack number development obtained from image processing of experiments.

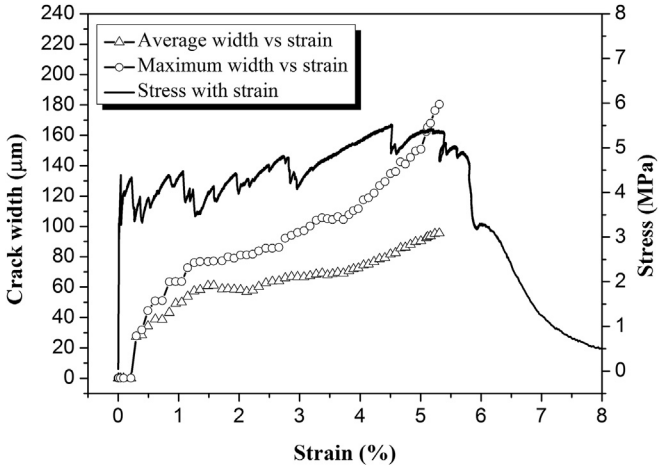

Fig. 15. Development of average width for all crack, width for largest crack as well as the applied stress with increasing strain.

From the figure, there is a rapid increase in crack number after the occurrence of the first crack (at roughly 4.3 MPa), but the number approaches a constant value when the applied stress is beyond about 5.0 MPa. In other words, the multiple cracking has reached the saturation state at around 5.0 MPa and few new cracks will form afterwards. This observation is consistent with the theory of multiple cracking in fiber reinforced brittle matrix composites. As mentioned in the introduction, for a new crack to form, there needs to be a sufficient distance from an existing crack for the fiber to transfer stress back to the matrix so the tensile strength of the matrix is reached again. Once the crack spacing reaches a value between the transfer distance and twice its value [16], no new cracks will be formed and the situation of saturated cracking is attained. Further increase in applied stress will simply result in increased opening of each crack.

4.2. Crack width development

In conventional tensile tests of SHCC, the tensile stress vs strain relation is measured to reflect the ductility of the material. With the processed image and following the procedure described in section 3.5, the average crack width within a cracking region and maximum crack width (i.e., the maximum averaged value among all regions) can also be determined. In Fig. 15, the average and maximum crack width is plotted against the strain. In the same plot, the stress vs strain relation is also shown. Unlike the crack number which approaches a constant value at saturation, the crack widths continue to increase until the localization of one major crack. From the results in Fig. 15, the crack width may show a slight decrease with increasing strain over part of the curve. This is an experimental error due to imperfect illumination condition during the measurement.

The results on crack width vs strain is of high practical significance. The width of cracks govern the transport properties of deformed concrete members and thus have a direct impact on durability [5]. Various investigations [6,17,18] have shown that the crack widths are more important than crack number when concrete durability is of concern. According to results in the literature [6,19,20], water permeability and chloride diffusivity of concrete are not affected by fine cracks with size smaller than around 60 μm. Because test results on cracked concrete in these studies are presented in terms of the average crack width, the curve of average crack width vs strain provides information on the effect of cracking (which can be negligible) when the material is under a given strain. On the other hand, the maximum crack width at a particular strain provides an idea of the worst situation. From our results, at a strain level of 0.5%, which is above the strain in common structural members at the serviceability state, the average crack width is roughly 35 μm while the maximum crack width is 45 μm. The tested SHCC should therefore be able to maintain the transport properties of the virgin material under normal loading conditions, so durability will not be affected. However, if there is a sudden overloading resulting in a permanent deformation of around 2% in the material (Note: for the sake of discussion, we assume the crack width vs strain relation to be similar under loading and unloading.), the maximum crack width becomes 81 μm, which will have effects on the transport properties and durability. From the curves of maximum and average crack width vs strain in Fig. 15, one can see that the two values can differ quite significantly at a particular strain. To quantify the variation in crack width, statistical

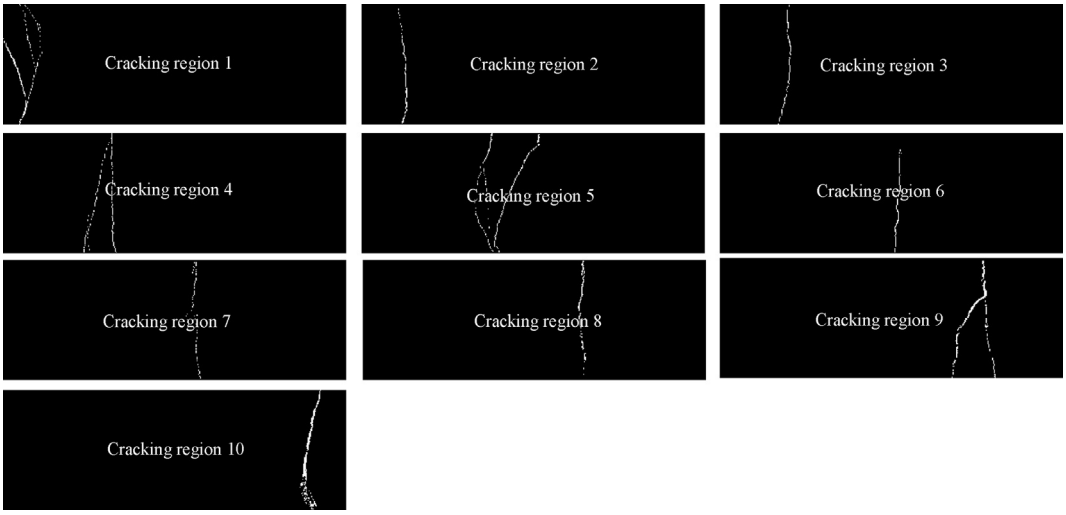

Fig. 16. Division of processed image into 10 cracking regions.

information will be obtained in the next sub-section.

4.3. Variation of average crack width between cracking regions

From the overall image, ten cracking regions were identified and they are shown in Fig. 16. As stated before, a cracking region may include one single crack (e.g., cracking region 2), a crack with several branches (e.g., cracking region 1) or closely located cracks that are connecting (cracking region 5).

To obtain statistical information, the average crack width in each cracking region is first obtained at different levels of applied strain. The results for a few representative strain values are plotted in Fig. 17, and significant variation in crack width can be observed. At each strain, the mean crack width is calculated as the weighted average of crack width for each region, with the weighting equal to the total crack length in each region. This way, the mean value is the same as that in Fig. 15, which is calculated by considering all the cracks together. Similarly, the weighted standard deviation can be obtained. The variations of mean value and standard deviation of crack width with applied strain are plotted in Fig. 18. For a member

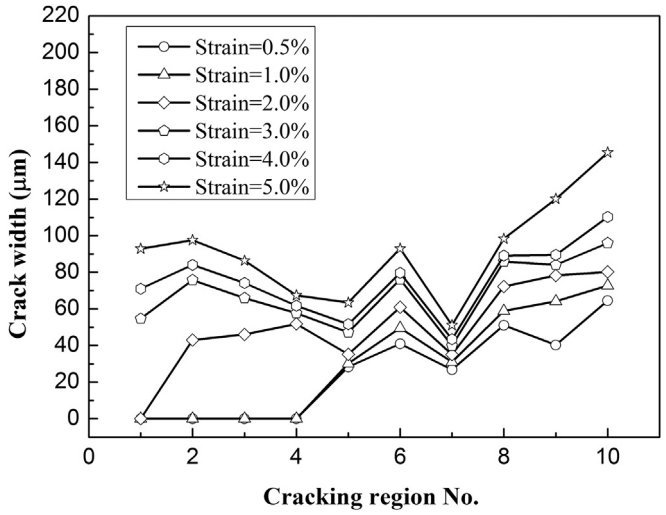

Fig. 17. Widths of all the ten cracking regions when strain equals to 0.5%, 1%, 2%, 3%, 4% and 5% respectively.

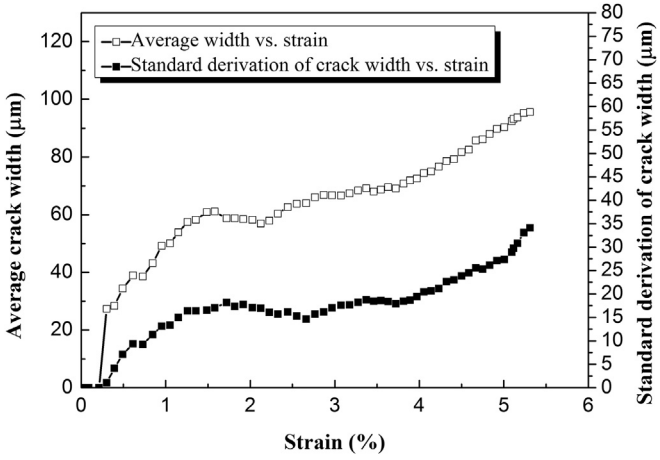

Fig. 18. Variation of mean value and standard deviation of crack width with strain.

under a given strain, one can then easily calculate the probability for the crack width to go beyond a certain critical value (say 60 μm). This can be a first step towards the risk-based durability design of members made with SHCC.

The standard derivation is around 20 μm from 1% to 4% strain. After 4%, the derivation increases to 35 μm since localization starts to occur at a particular crack which continues to open while the other cracks stay essentially unchanged.

A physical explanation for the large variation in crack width among different regions of the specimen is the difference in crack bridging behavior, which is related to the distributions of flaw size and fiber in different sections of the member. On one hand, the variation of flaw size has a major influence on the cracking strength of matrix [1] and it can be revealed by the technique of X-ray computed tomography (μCT) method [21]. Along with image processing method described in the current study, the cracking strength for each crack can be observed and then correlated with the flaw size measured by μCT method. This work will be covered in a separate publication under preparation. On the other hand, the post-crack bridging behavior is mainly dependent on the fiber distribution. During the mixing and casting process, inevitable inhomogeneity in fiber distribution will be introduced, resulting in a fluctuation of fiber number and inclination angle from one section

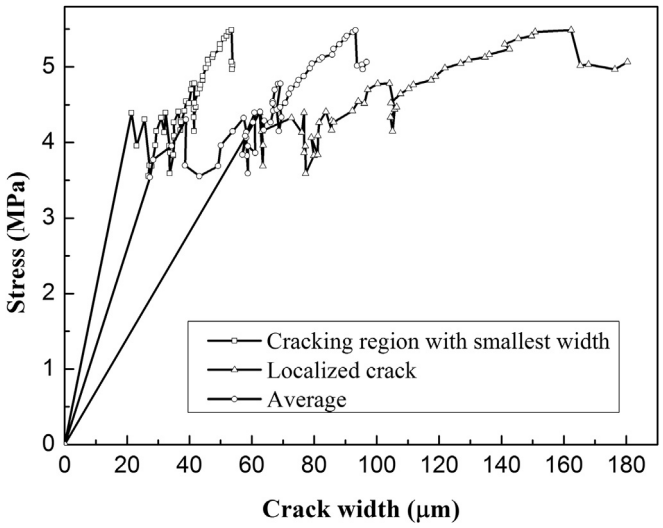

Fig. 19. Cracking region with smallest width, localized crack and average crack width.

to another. Such variation is expected to be more severe for high fiber content due to fiber dispersion issue. As the ultimate tensile strength dependent on the peak bridging stress of the weakest plane, a higher variation will make the tensile strength lower. Furthermore, with varying number and inclination angle of bridging fibers, the crack width corresponding to the same stress will be very different from one section to another. In the literature, fluorescence technique [51] has been used to obtain the fiber distribution in terms of both the fiber count and inclination angle from cut cross-sections of SHCC. As the image processing method described in this study can experimentally determine the bridging law of a cracking plane (examples are shown in Fig. 19), it can be incorporated to investigate the influence of fiber distribution on the cracking behavior of SHCC, which is of major interest in further investigations.

5. Conclusions

For strain hardening cementitious composites (SHCC), the multiple cracks often exhibit complex patterns, with high variation in crack width. In this study, a new double-threshold algorithm was first developed to treat large and small cracks separately, so all crack widths can be accurately captured. The approach has been verified by comparing crack width from a processed image to direct measurements under the microscope. Then, another algorithm was developed to automatically eliminate noises in the image and separate cracking regions from one another. By processing sequential images taken from the same specimen, the development of the cracking patterns with increased loading can be tracked and useful information can be obtained.

The crack number from image processing is found to show a reasonable trend consistent with theory of stress transfer. At various strain levels, the mean crack width and standard derivation are assessed, so the probability for a crack to exceed a critical width can be determined to facilitate durability design.

Acknowledgement

Financial support of this work by the Hong Kong Research Grant Council through Project 615411 is gratefully acknowledged.

References

[1] V.C. Li, C.K.Y. Leung, Steady-state and multiple cracking of short random fiber composites, J. Eng. Mech. 118 (11) (1992) 2246–2264.
[2] V.C. Li, From Micromechanics to Structural Engineering-the Design of Cementitious Composites for Civil Engineering Applications, 1993.
[3] C.K.Y. Leung, Design criteria for pseudoductile fiber-reinforced composites, J. Eng. Mech. 122 (1) (1996) 10–18.
[4] T. Kanda, V.C. Li, Effect of fiber strength and fiber-matrix interface on crack bridging in cement composites, J. Eng. Mech. 125 (3) (1999) 290–299.
[5] E.-H. Yang, S. Wang, Y. Yang, V.C. Li, Fiber-bridging constitutive law of engineered cementitious composites, J. Adv. Concr. Technol. 6 (1) (2008) 181–193.
[6] K. Wang, D.C. Jansen, S.P. Shah, A.F. Karr, Permeability study of cracked concrete, Cem. Concr. Res. 27 (3) (1997) 381–393.
[7] M. Lepech, V.C. Li, Water permeability of cracked cementitious composites, Proc. Eleventh Int. Conf. Fracture (2005) 20–25.
[8] H.C. Wu, V.C. Li, Snubbing and bundling effects on multiple crack spacing of discontinuous random fiber-reinforced brittle matrix composites, J. Am. Ceram. Soc. 75 (12) (1992) 3487–3489.
[9] C. LU, C.K.Y. Leung, A new model for crack spacing and ductility in SHCC, in: E. Schlangen, M.G. Sierra Beltran, M. Lukovic, G Y (Eds.), RILEM SHCC3, RILEM S. A. R. L, Dordrecht, 2014, pp. 259–266.
[10] E.B. Pereira, G. Fischer, J.A. Barros, Direct assessment of tensile stress-crack opening behavior of Strain Hardening Cementitious Composites (SHCC), Cem. Concr. Res. 42 (6) (2012) 834–846.
[11] M. Maalej, V.C. Li, T. Hashida, Effect of fiber rupture on tensile properties of short fiber composites, J. Eng. Mech. 121 (8) (1995) 903–913.
[12] C.J. Adendorff, W.P. Boshoff, Zijl Gv, Characterisation of Crack Distribution of Strain-hardening Cement Composites (SHCC) under Imposed Strain, CRC Press, 2009, pp. 215–221. Advances in Cement-Based Materials.
[13] C. Wagner, N. Bretschneider, V. Slowi, Evaluation of crack patterns in strain hardening cement-based composites (SHCC) with respect to structural durability, Restor. Build. Monum. 17 (3/4) (2011) 221–236.
[14] C. Wagner, A. Dollase, V. Slowi, Evaluation of crack patterns in SHCC with respect to water permeability and capillary suction, in: A.L. . Ae (Ed.), Concrete Repair, Rehabilitation and Retrofi Tting III, 2012.
[15] Y. Fujita, Y. Mitani, Y. Hamamoto, A Method for Crack Detection on a Concrete Structure. Pattern Recognition, 2006 ICPR 2006 18th International Conference on, IEEE, 2006, pp. 901–904.
[16] J. Aveston, R.A. Mercer, J.M. Sillwood, Fiber Reinforced Cements-scientific Foundations for Specifications. Composites-standards, Testing and Design Guildford, Surrey, U. K.: National Physical Laboratory IPC Science and Technology Press Ltd, 1974, pp. 93–103.
[17] H.-W. Reinhardt, M. Jooss, Permeability and self-healing of cracked concrete as a function of temperature and crack width, Cem. Concr. Res. 33 (7) (2003) 981–985.
[18] M. Sahmaran, V.C. Li, Engineered Cementitious Composites: Can Composites Be Accepted as Crack-free Concrete?, 2010.
[19] A. Djerbi, S. Bonnet, A. Khelidj, V. Baroghel-Bouny, Influence of traversing crack on chloride diffusion into concrete, Cem. Concr. Res. 38 (6) (2008) 877–883.
[20] S.Y. Jang, B.S. Kim, B.H. Oh, Effect of crack width on chloride diffusion coefficients of concrete by steady-state migration tests, Cem. Concr. Res. 41 (1) (2011) 9–19.
[21] S. Fan, M. Li, X-ray computed microtomography of three-dimensional microcracks and self-healing in engineered cementitious composites, Smart Mater. Struct. 24 (1) (2014) 015021.